Plasma Sources Sci. Technol. **17** (2008) 035006 (11pp) doi:10.1088/0963-0252/17/3/035006

Dynamics of fireballs

R L Stenzel[1], C Ionita[2] and R Schrittwieser[2]

[1] Department of Physics and Astronomy, University of California, Los Angeles, CA 90095-1547, USA
[2] University of Innsbruck, Department for Ion Physics and Applied Physics, A-6020 Innsbruck, Austria

E-mail: stenzel@physics.ucla.edu

Received 16 January 2008, in final form 18 January 2008
Published 23 May 2008
Online at stacks.iop.org/PSST/17/035006

Abstract
Fireballs are discharge phenomena on positively biased small electrodes in plasmas. The discharge arises from electron energization at a double layer. Fireballs can collect relatively large electron currents from the ambient plasma. Fireballs can become unstable to relaxation oscillations. This paper addresses the space–time evolution of pulsed fireballs. Growth and collapse of fireballs produce large density and potential variations near the electrode which couple into the background plasma production. Unstable fireballs emit bursts of fast ions and ion acoustic waves. High-frequency emissions near the electron plasma frequency have been observed and associated with the sheath–plasma instability rather than electron beam–plasma interactions. New shapes of fireballs have been observed in dipole magnetic fields.

(Some figures in this article are in colour only in the electronic version)

1. Introduction

Introducing a biased electrode into a plasma produces a great variety of phenomena which have been studied by many researchers. Early work focused on the current–voltage characteristics of plane probes for purpose of plasma diagnostics [1, 2]. Plane probe theories were extended to include different probe geometries [3]. The work advanced to include time dependence [4,5], magnetic field effects [6,7], effects of collisions [8], ion beams [9,10], secondary electron emissions [11] and sheath–plasma instabilities [12]. It was also recognized that drawing currents from the plasma perturbs the plasma and produces various instabilities such as ion acoustic [13] and ion cyclotron waves [14]. In a magnetic field a finite-size electrode can also produce ion cyclotron oscillations due to perpendicular ion acceleration [15,16] and similar relaxation instabilities due to periodic expulsion of unmagnetized ions across field lines [17]. For pulsed electrodes the current flow within the plasma has been investigated. The current is carried by an electromagnetic eigenmode of the plasma such as the whistler [18] or Alfven mode [19]. Current closure involves the external circuit with return current electrode [20]. Current disruptions within the plasma produce inductive voltages in the external circuit [21] leading to double layers inside the plasma [22]. Anode double layers can also arise from ion beam reflections [10,23] and from ionization phenomena near the electrode, called fireballs.

Anode fireballs are discharge phenomena near positively biased electrodes. These are highly nonlinear phenomena involving the physics of sheaths, double layers, ionization, beams and possibly external circuit interactions. These phenomena have been studied by many investigators [24–29]. Much of the attention has been focused on the formation of double layers [30], the current–voltage characteristics and the relaxation oscillations of unstable fireballs, which have been analyzed in the framework of chaos theory [31]. Fundamental questions remain with respect to the peculiar shapes of fireballs, the physics of the relaxation oscillations including waves and instabilities created by non-Maxwellian distribution functions, both in unmagnetized and magnetized plasmas. The present experiment addresses some of these questions with a new approach, i.e. to pulse the electrode voltage. Space- and time-resolved measurements of plasma properties, light emission and waves have been performed. These show the growth and decay of fireballs in different gases with and without magnetic fields, the plasma dynamics, ion beams, ion acoustic and electron plasma waves.

The paper first describes the experimental setup and diagnostics. Then the basic physics of fireballs is presented. Experimental results on plasma dynamics, light emission, ballistic and ion acoustic waves, and oscillations near the electron plasma frequency are described. A conclusion describes the new findings and implications on fireball shapes.

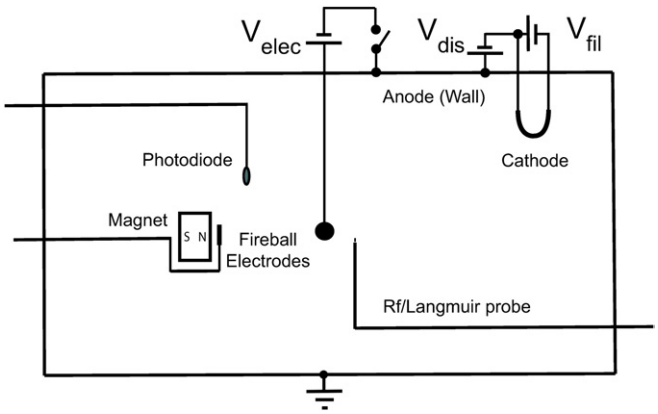

Figure 1. Schematic of the experimental setup.

2. Experimental setup

The experiments are performed in the Innsbruck DP-machine without separating grid [31], a cylindrical vacuum chamber (0.45 m diameter, 0.9 m length) with surface magnets for primary electron confinement, schematically shown in figure 1. An unmagnetized discharge plasma (density 10^8–10^9 cm^{-3}, electron temperature $kT_e \simeq 2$ eV) is produced in argon, neon and hydrogen at pressures 1–5 mTorr. Fireballs are created by inserting a spherical electrode (1 cm diameter) into the unmagnetized plasma or a planar disc (one-sided, 1 cm diameter) in front of a strong permanent magnet (0.2 T max) for studying magnetized fireballs. A spherical electrode geometry in an unmagnetized plasma was thought to produce concentric fireballs, which was not the case.

Plasma diagnostics consist of a movable, coax-fed cylindrical Langmuir probe (0.5 mm diameter, 3 mm length, 50 Ω coax with 2 mm diameter) which is also used for measuring ion acoustic and electron plasma waves. The current–voltage characteristics of a cylindrical probe show no sharp knee at the plasma potential and no electron saturation current, hence the measured current depends on density, temperature and plasma potential. For measuring ion acoustic waves the probe is positively biased (100 V) and ac coupled with an RC network or a broadband transformer (0.1–10 MHz). For detecting signals in the regime of the electron plasma frequency the rf probe is fed into a tuned rf amplifier (Boonton 230A, 10–500 MHz, 30 dB), rectified with a square-law crystal detector and the rf power displayed on a digital oscilloscope. An emissive probe is available for measuring the plasma potential [32]. A photodiode is used for time- and space-resolved light measurements. Rise and fall time constants of $\tau = 0.77\,\mu$s are measured in response to a pulsed light-emitting diode. The photodiode is used both outside the plasma for spatially integrated light measurements and inside the chamber, mounted on a movable probe shaft, to resolve the axial light profile. Finally, a digital camera is used to take time-averaged images of fireballs.

In order to study the fireball dynamics, i.e. growth, decay and instabilities, the electrode voltage is pulsed with fast transistor switch (<0.1 μs rise and fall times). Pulse width and repetition rate are widely adjustable.

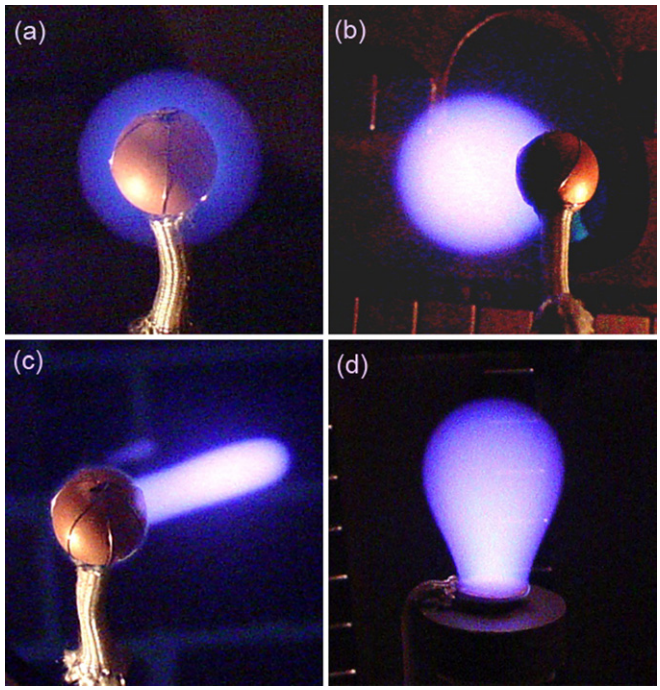

Figure 2. Fireball shapes: (*a*) luminescent sheath, (*b*) Spherical fireball, (*c*) Cylindrical fireball and (*d*) pear-shaped fireball in a dipole magnetic field.

3. Experimental results

3.1. Basic fireball formation

In order to create a fireball we first produce a dc discharge with the heated tungsten cathode ($V_{fil} = 6.5$ V, $I_{fil} = 7$ A) biased negatively ($V_{dis} \simeq -50$ V, $I_{dis} = 0.1$ A) with respect to the grounded chamber wall, which forms the anode. Typical plasma parameters are a density $n_e \simeq 10^8$ cm^{-3}, $kT_e \simeq 2$ eV, in argon at a pressure of 3 mTorr.

With increasing electrode voltage first a visible sheath is observed around the electrode (see figure 2(*a*)) The visible sheath is concentric with the spherical electrode and a few millimeters thick. The light emission is produced by excitation of neutrals ($n_0 \gg n_e$) due to collisions with energetic electrons (>10 eV). Since there is little light outside the sheath the electrons must have gained their energy in the sheath, and hence are not primary electrons from the cathode. Collecting electrons from the plasma also requires a larger ion flux to the chamber wall, accomplished by an increase in the plasma potential in the entire chamber. With increasing electrode voltage the faintly visible sheath changes abruptly to a bright glow of spherical, ellipsoidal or cylindrical shape, called a 'fireball' (see figures 2(*b*) and (*c*)). This sheath instability is well known from earlier experiments and theories [33,34]. The dimensions of the fireball (1–3 cm diameter) are larger than that of the electrode sheath. The sharp boundary of the fireball indicates a local acceleration region well outside the sheath, which has been identified in many previous experiments as a double layer [28, 29, 31, 35]. The fireball attaches itself to the side of the electrode. The location does not depend on surface irregularities since rotation of the sphere does not affect the position of the fireball. Neither have the location,

shape and size of the fireballs been fully explained previously. In the presence of a magnetic field the fireball becomes predictably field-aligned [26]. In a non-uniform dipole field the combination of a cylinder and a sphere leads to a pear-shaped fireball (figure 2(*d*)). The observation of a cylindrical fireball in the absence of a magnetic field is new and interesting. Radially accelerated electrons mostly traverse the fireball since there is no significant electric field within the fireball and the electron mean free path exceeds the fireball diameter. The existence of this shape also implies perfect radial momentum balance between counter-streaming electrons and ions.

When a fireball is created the discharge voltage can be decreased to zero since the positively biased electrode becomes the anode. This simplifies the physics of the device: the primary electrons emitted by the filament are collected by the electrode rather than the chamber wall which has the same potential as the cathode. Secondary electrons due to ionization of neutrals by primaries are also collected by the electrode. Since the plasma potential is very positive the ions are collected by the chamber wall (cathode surface is negligible). The primary electron energy is determined by the plasma potential which is close to the electrode potential, $V_{\rm plasma} \simeq V_{\rm elec} - V_{\rm dl}$ where the double layer potential is approximately the ionization potential, $V_{\rm dl} \simeq 15\,{\rm eV}$ in Ar and $\simeq$24 eV in Ne. The primary electrons have a short mean free path for elastic collisions with neutrals. The secondary electron density is much larger than the primary electron density. In order to maintain space–charge neutrality the loss of secondary electrons and ions must be equal.

Both primary and secondary electrons are collected at the double layer. In entering the fireball the primary electrons gain relatively little energy and hence should produce little contrast in light emission. Thus, the bright fireball must arise from the collection of secondary electrons that are energized from 2 eV, which produces no light, to an energy of $>$15 eV when light is excited. The current collected by the fireball or electrode is dominated by the collection of secondary electrons. The electrode current is the sum of the cathode current and the ion current to the chamber wall. The division of current between different groups of charged particles must be accomplished by internal electric fields. When the chamber wall is floating the anode and cathode currents are exactly equal. This mode of operation is only possible in the presence of a plasma since it is difficult to start the discharge with a large separation between anode and cathode. Lastly, fireballs have also been created in a slowly decaying afterglow plasma where no primary electrons are present [5]. In this case the electron current collected by the fireball equals the ion current collected by the chamber wall. In any case fireballs are subject to current-limitations imposed by the ambient plasma.

The energized secondary electrons produce both excitation and ionization inside the fireball. In pulsed operation the ionization starts inside the sheath. Electrons are quickly accelerated to the electrode, ions are slowly moving away from the electrode, leaving a temporary excess of ions in an initially electron-rich sheath. A double layer evolves. The potential profile separates into a sheath and a double layer outside the sheath. The same physics holds when an incident ion beam is reflected inside an electron-rich sheath [9, 10, 23]. The sheath expands and forms a double layer. In non-planar geometries the sheath expansion leads to an increase in surface area for collecting of electrons, hence the electrode current increases. The current increase due to the density enhancement by ionization is minimal since in case of a stationary double layer the collection of newly created electrons cannot exceed the ion flux out of the fireball which is minimal, $I_{\rm ion}/I_{\rm el} \simeq (m_{\rm e}/m_{\rm i})^{1/2}$.

The outflow of excess ions leads to an expansion of the double layer and a rise in the electrode current. The growth of the fireball is limited by two factors: (i) the electrode current cannot exceed the temperature-limited emission current from the cathode. (ii) The spherical expansion of the excess ions leads to a density decrease and weakening of the double layer. A steady state may be achieved when the outward streaming ions are replaced by new ions at the same rate. Otherwise the double layer will collapse and revert to an electron-rich sheath at the electrode. The decrease of both electrode and cathode current leads to a density drop. The process repeats leading to a pulsating or unstable double layer. These considerations show that there is a strong coupling between the two ionization regions. The fireball cannot be analyzed separately but is part of a closed current system.

When the electrode voltage is pulsed a fireball cannot be created without a background plasma. The reason is that in vacuum the cathode emission is space–charge limited, which is negligibly small in comparison with the temperature-limited emission in a plasma. If pulsed fireballs are created at a sufficiently fast repetition rate the afterglow plasma from one fireball is sufficient to ignite the next one and no background plasma source is required. The density rise in the discharge leads to a delayed onset of the fireball. This may also explains the long repetition time in some unstable fireballs.

Another simplification is to operate the discharge at a constant voltage so as to eliminate instabilities associated with the external circuit. It is well known that external R,L,C circuits produce relaxation oscillations in conjunction with a nonlinear device with negative differential resistance. In this work we are only interested in instabilities inside the plasma, hence do not insert series resistances between the electrode and voltage source.

3.2. Electrode current, fireball light

The formation of fireballs depends on many parameters (electrode voltage and current, discharge current and voltage, neutral gas type and pressure, pulse length and repetition rate) and therefore produces a variety of effects. In particular the stability of fireballs can vary considerably. Some examples of stable and highly unstable currents are shown in figure 3. When a constant voltage pulse is applied to the electrode the rise in the electrode current, i.e. fireball formation, occurs with a delay which depends on plasma density. In pulsed mode without discharge voltage the repetition rate determines the background density. Figure 3(*a*) shows an increasing delay with increasing repetition time. The delay arises from a slow build-up of density in the large plasma chamber. The cathode current increases as the density builds up because the cathode

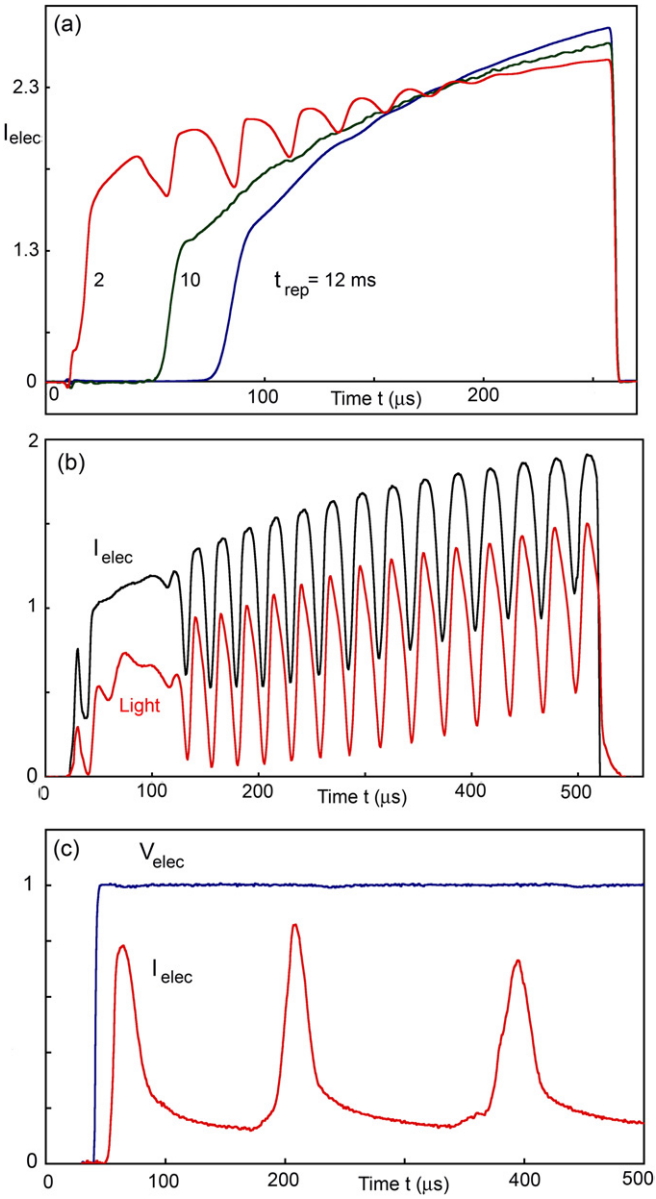

Figure 3. Typical waveforms of current, light and voltage for fireballs. (*a*) Electrode currents in an unmagnetized Ar plasma for different pulse repetition times. No background discharge is provided ($V_{dis} = 0$). The fireball onset and stability depends on the background density which decreases with increasing repetition time ($V_{elec} = 58$ V, $I_{elec,max} \simeq 0.2$ A, pulse width 250 μs, 2.8 mTorr Ar). (*b*) Electrode current and light emission in a magnetized Argon plasma (4 mTorr, $V_{dis} = 20$ V, $V_{elec} = 55$ V, $t_{rep} = 1$ ms). Note the delayed onset of a strong instability which partly disrupts the current and light emission. Its frequency decreases from 41.7 to 32.3 kHz. After current switch-off the light decreases with a decay time $\tau = 6\,\mu$s. (*c*) Electrode voltage and current in a neon plasma ($p = 7$ mTorr, $V_{elec} = 80$ V, $V_{dis} = 30$ V, $t_{rep} = 1$ ms, $I_{dis,max} = 180$ mA). The fireball is highly unstable with short current pulses and long repetition times which are determined by the plasma dynamics in the chamber rather than in the fireball.

sheath decreases and the electric field increases. Since the peak current does not depend on the initial density or pulse repetition time, the plasma density must have recovered to similar values in all three cases. For a low initial density this process takes longer. The increased current allows ionization in the anode

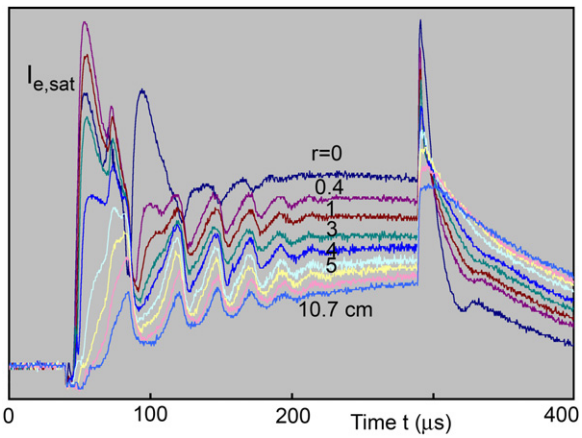

Figure 4. Electron saturation current versus time at different radial distances from the fireball center. The electrode voltage is pulsed on at $t \simeq 40\,\mu$s for 250 μs. ($V_{elec} \simeq 60$ V, probe bias $V_{pr} = 100$ V).

sheath and the formation of a fireball. The fireball is formed on a much shorter time scale than the delayed density build-up in the plasma volume. The current rises due to continued ionization. The current may exhibit a transient oscillation before reaching a steady state.

However, the current may also become unstable, as shown in figure 3(*b*). In pulsed mode it is possible to determine the growth rate of the instability, but it is often comparable to the oscillation period. The current is periodically disrupted but not enhanced. The limiting peak current gradually increases by ionization. The oscillation frequency slightly decreases in time (42–32 kHz). The light emission from the fireball has been measured with a photodiode mounted outside the chamber at a window, thus integrating the light over the entire fireball. The light indicates the presence of a fireball. Current disruption and loss of the fireball are strongly correlated although the cause–effect relation remains to be determined. It is also interesting to note that the light emission decays slowly ($\tau \simeq 6\,\mu$s) after switch-off of the electrode current. The time response of the photodiode is fast enough to resolve the energy decay of the energetic fireball electrons. The hot electrons cannot leave the fireball faster than the ions but can transport heat rapidly. The finite light decay time also implies that the fireball may actually not exist at the light minima.

Finally in figure 3(*c*) we show a highly unstable fireball in a neon plasma. In spite of a constant voltage applied to the electrode the current consists of a sequence of pulses with repetition time ($t_{rep} \simeq 200\,\mu$s) much larger than the pulse width ($\Delta t \simeq 25\,\mu$s). The former may be related to an ion transit time across the device, the latter across the radius of the fireball. Visual inspection shows a fuzzy fireball without sharp boundaries, which is the result of the periodic expansion and contraction of the fireball. Since Ne has a higher ionization potential (21.6 eV) than Ar (15.5 eV) or H_2 (13.6 eV) a higher electrode and discharge voltage are needed to produce discharges and fireballs.

3.3. Plasma dynamics

We now turn to the dynamics of pulsed and unstable fireballs as measured with a Langmuir probe. Figure 4 shows the time

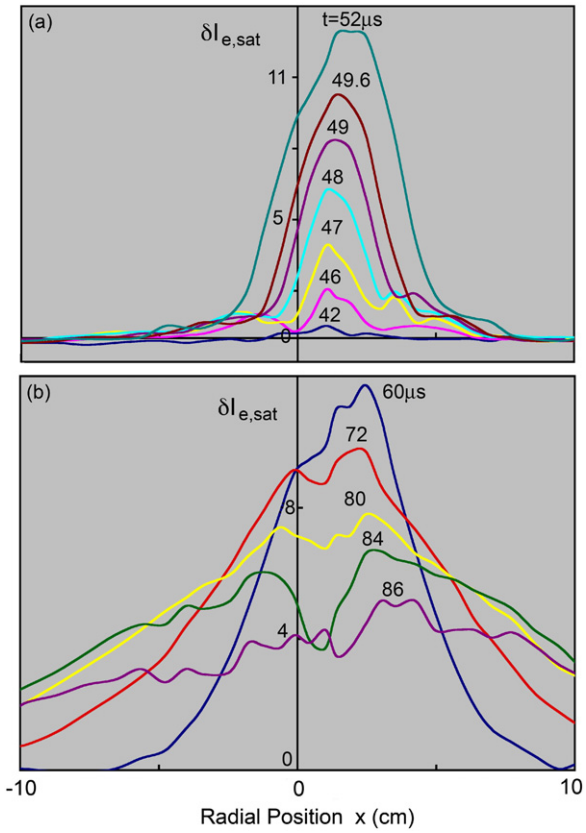

Figure 5. Electron saturation current versus radial position at different times during (*a*) the growth of the fireball and (*b*) its first collapse ($r = 0$ is the machine axis through the spherical electrode, axial probe position $\Delta z \simeq 0.5$ cm in front of electrode surface). The constant electrode voltage $V_{\rm elec} = 80$ V is pulsed on at $t = 40\,\mu$s and off at $t = 280\,\mu$s (see figure 4). Note the growth of a localized plasma near at the electrode, its broadening and the collapse of the plasma near the electrode during the first current disruption.

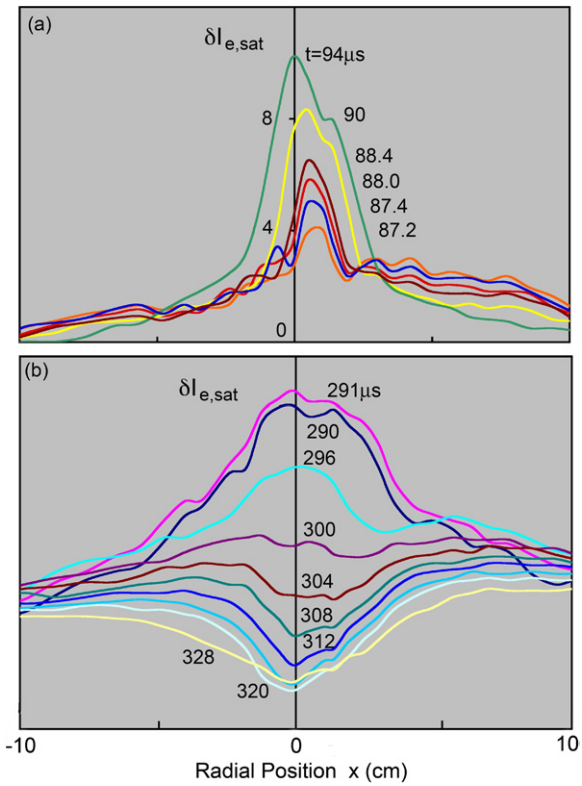

Figure 6. Electron saturation current versus radial position at different times during (*a*) the second growth of the fireball and (*b*) the response to switching the electrode voltage off. The re-growth of the fireball due to its inherent current instability is similar to that of the switch-on of the electrode voltage. Thus current disruptions are like switched fireballs. Likewise the collapse of the central fireball after voltage switch-off is similar to the collapse during natural current oscillations, i.e. a temporary density depletion is formed (see figure 5(*b*)).

dependence of the ac coupled (0.3 μF, 10 kΩ, RC = 3 ms) electron saturation current versus time at different radial distances r from the axis of the machine. The axial probe position is $\Delta z \simeq 0.5$ cm in front of the electrode where the fireball is centered. Inserting the probe into the fireball causes its position to shift, hence data interior to the fireball may be underestimated. The electrode is pulsed ($V_{\rm elec} \simeq 60$ V for 250 μs) in an unmagnetized Ar discharge (3 mTorr). As the electrode voltage is applied ($t \simeq 40\,\mu$s) the electron saturation current increases near the electrode due to electron heating and density increase by ionization. The electrode current exhibits disruptions which decay in time similar to those shown in figure 3(*a*) for $t_{\rm rep} = 2$ ms. The current disruptions change the probe current well away from the fireball. Non-propagating current perturbations are due to plasma potential variations. For example, when the electrode current increases the plasma potential outside the double layer drops by the ionization potential which causes an increase in the saturation current of the cylindrical probe. Vice versa, the probe current drops when the double layer collapses. Especially obvious is this effect when the electrode voltage is switched off. The plasma potential abruptly decreases and the probe current dramatically increases. Well after switch-off, neglecting temperature and potential changes, one can estimate the density decay time, $\tau_n \simeq 1.5$ ms.

At a given time we now plot the saturation current versus radial distance. Figure 5(*a*) shows two phases of the fireball, (*a*) its growth and (*b*) its collapse. The probe current shows a rapid growth close to the electrode, slightly off center since the fireball forms at a side of the spherical electrode. Since $I_{\rm e,sat} \propto n(kT_{\rm e})^{-1/2}$ the increase reflects heating and ionization, but may underestimate the effects inside the fireball where the plasma potential increases, causing a decrease in the probe current. Outside the fireball electron heating and potential gradients should be minimal such that the probe current indicates the real density profile. In time the radial profile broadens, i.e. the fireball radius increases.

The next phase is the disruption of the fireball depicted in figure 5(*b*). The enhanced density and temperature of the fireball collapse and turn into a minimum. Since in the absence of the fireball large radial temperature and potential variations are unlikely the current minimum indicates a true density minimum. Without ionization the ion outflow has created a density hole where the fireball was located. Further below we will show direct observations of ion ejection from the fireball.

We show next the self-consistent recovery of the fireball. Figure 6(*a*) shows again a rapid growth of density and

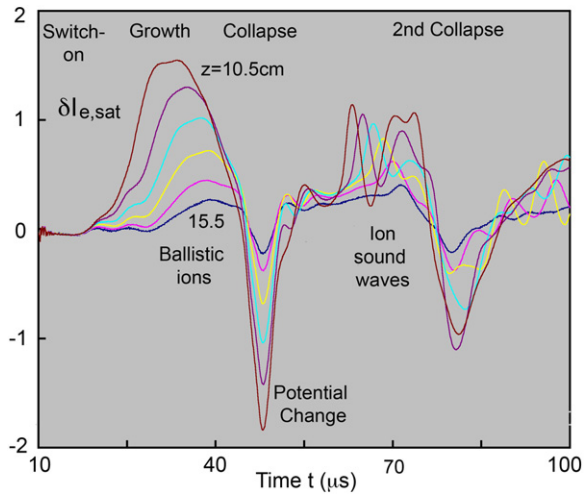

Figure 7. Perturbation of the electron saturation current versus time at different axial positions z from the electrode. The electrode voltage $V_{\rm elec} = 65$ V is switched on at $t = 10\,\mu$s for 500 μs, $t_{\rm rep} = 4$ ms. The fireball is unstable and has its first disruption at $t \simeq 48\,\mu$s, a second disruption at $t \simeq 82\,\mu$s. Propagating perturbations are ion bursts or ion acoustic waves, space-independent perturbations are interpreted as plasma potential changes. Argon, 2.7 mTorr. $V_{\rm dis} = 0$, $I_{\rm elec} = 70$ mA.

temperature. It is similar to that at turn-on of the electrode voltage. The peak occurs slightly to the left of the previous maximum, indicating that the fireball location may shift slightly from pulse to pulse or be non-spherical until steady state is reached. All subsequent fireball growths and disruptions have a similar character as the first ones, but as seen from figure 4 the instabilities die out in time and a steady-state fireball evolves.

Finally we show in figure 6(*b*) the effect of abruptly switching off the electrode voltage and current. Measurements are done just after switch-off when the double layer is absent and the probe current highly reflects the density profile. The quasi steady-state profile (top trace) flattens and then inverts into a density depression near the electrode, presumably due to surface recombination at the floating electrode. Thus, when the electrode voltage is pulsed on again, the initial current collected will be smaller than the electron saturation current for a non-perturbing electrode.

3.4. Ion bursts and acoustic waves

After having shown the plasma production and losses in a pulsating fireball we now turn to the investigation of wave phenomena. For this purpose the ac component of the electron saturation current is analyzed. The probe is biased positively and the ac current is coupled out with a pulse transformer (10 mH). Time waveforms of $\delta I_{\rm e,sat}$ are recorded at different axial distances from the electrode.

Figure 7 shows some raw traces of $\delta I_{\rm e,sat}(t)$ outside the fireball. Several features can be observed: if a perturbation shows no delay it is caused by plasma potential changes. This occurs twice (48 μs, 80 μs) when the fireball collapses, the plasma potential rises and the current drops. During the first growth of the fireball (20–40 μs) a propagating enhancement in

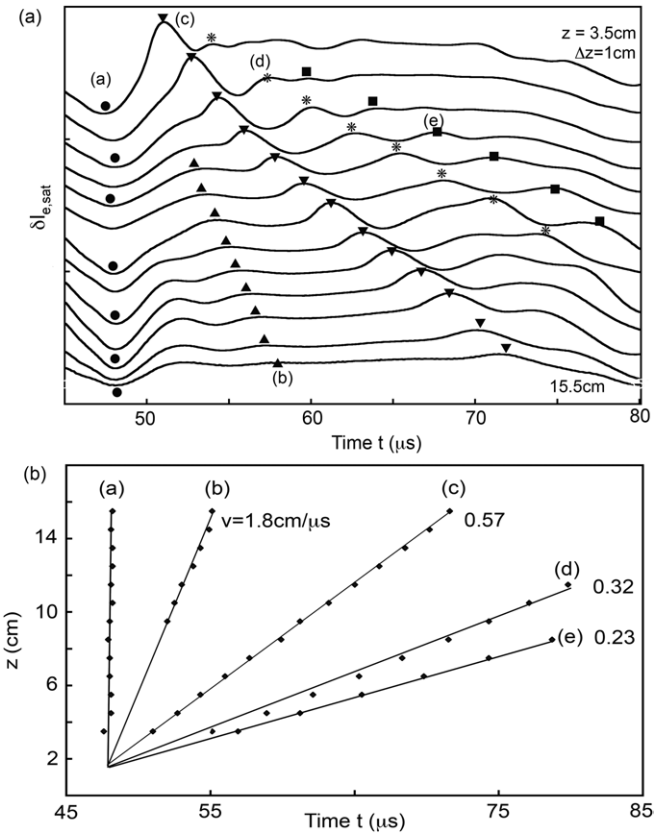

Figure 8. Time-of-flight diagram for the propagating density perturbations following the first disruption in argon. (*a*) Ac component of the electron saturation current versus time at different axial positions. (*b*) z–t diagram of perturbations in $\delta I_{\rm e,sat}$. The first perturbation is instantaneously present at all locations, hence is thought to be a global plasma potential change. The following perturbations (b–d) travel at supersonic speed and are interpreted as ballistic signals of streaming ions. The last perturbation travels at the ion acoustic speed for $kT_{\rm e} = 2$ eV.

the saturation current is observed. The peak propagates axially with an initial speed of $v_z \simeq 4.6 \times 10^5\,{\rm cm\,s^{-1}}$. Since the ion acoustic speed in Ar at $kT_{\rm e} = 2$ eV is $c_{\rm s} = 2.2 \times 10^5\,{\rm cm\,s^{-1}}$ the propagating feature must be a ballistic signal of streaming ions with energy 8.6 eV.

After the collapse of the fireball several fast oscillations are detected. Their properties are displayed in a time-of-flight diagram shown in figure 8. Traces of $\delta I_{\rm e,sat}(t)$ at different axial positions, suitably offset, are presented in figure 8(*a*) while the z–t trajectory of some pronounced features are shown in figure 8(*a*). The first depression (a) again indicates the collapse of the fireball. It is followed by a sequence of propagating features (b–d) which are supersonic and interpreted as ballistic ion signals. Only the last oscillation (e) travels at the sound speed which has also been seen in earlier experiments [36]. For an approximate period of 5 μs the wavelength would be 1.2 cm. The major ballistic mode (c) corresponds to an ion streaming energy of $(5.7/2.2)^2 \times 2 = 12.9$ eV which is close to the double layer potential [37]. The first ballistic mode (b) may be a light ion impurity since the kinetic energy for Ar would exceed the electrode potential. If it had the same energy as Ar the mass would be $(5.7/18)^2 \times 40 = 4$, hence the impurity

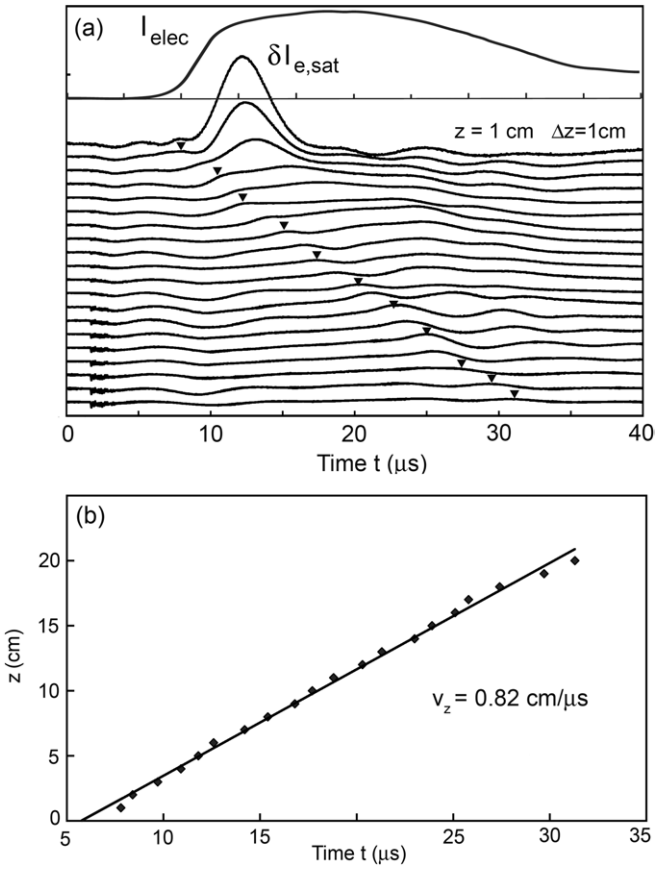

Figure 9. Time-of-flight measurements of Ne ions in a pulsed, unstable fireball. (*a*) Electrode current (top trace) and perturbations in the electron saturation current versus time at different axial positions z from the electrode. The large peak near the electrode is due to the formation of the fireball. (*b*) z–t diagram of the traveling perturbation in $\delta I_{e,sat}$. A least-squares fit indicates a propagation velocity $v_z = 0.82\,\mathrm{cm}\,\mu\mathrm{s}^{-1}$, corresponding to a streaming energy of 6.9 eV. Parameters: 7.3 mTorr Ne, $V_{elec} = 80$ V, $I_{elec,max} \simeq 100$ mA, $V_{dis} = 30$ V, $t_{pulse} = 0.5$ ms, $t_{rep} = 1$ ms).

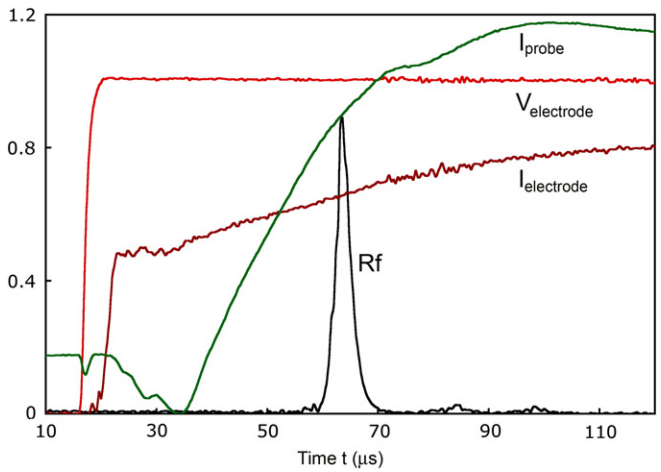

Figure 10. Turn-on of a stable fireball with electrode voltage and current, Langmuir probe current and 136 MHz rf signal. A sharp line is produced since the density increases at turn-on and the frequency scales with plasma frequency. ($V_{elec} = 63$ V, $I_{elec,max} \simeq 116$ mA, $V_{dis} = 26$ V, $t_{pulse} = 0.5$ ms, $t_{rep} = 1.1$ ms, 3.3 mTorr Ar).

would be He. All trajectories trace back to the fireball and start at the time of the collapse. In the presence of the double layer, ions are streaming continuously outward. The collapse of the accelerating potential terminates the stream and creates the traveling transient. Since the ion acoustic wave is also excited by the double layer collapse it is not due to instabilities associated with the ion beam or electron current. Interestingly, no comparably large ion transients are excited when the double layer builds up.

Similar time-of-flight measurements have been performed in a neon plasma where fireballs are notoriously unstable (see figure 3(*c*)). The focus here is on the ion dynamics at the time of fireball formation, i.e. just after the turn-on of the electrode voltage.

Figure 9(*a*) shows for timing reference the waveform of the electrode current (top trace) together with the perturbations in the electron saturation current $\delta I_{e,sat}(t)$ at different distances from the electrode, spaced 1 cm apart. The gain has been increased with distance to compensate for the signal loss by spherical expansion. The electrode voltage is applied at $t \simeq 2\,\mu$s and the rapid current rise occurs at $t \simeq 10\,\mu$s. Close to the electrode there is a large, non-traveling perturbation in $\delta I_{e,sat}$ which is due to the hot electrons formed inside the fireball. A traveling perturbation is observed for distances of up to 20 cm. Figure 9(*b*) shows a time-of-flight diagram which reveals the propagation speed is supersonic ($c_s = 3.1 \times 10^5\,\mathrm{cm\,s^{-1}}$ for $kT_e = 2$ eV) and hence should be a burst of streaming ions with kinetic energy $1/2 m_i v^2 = 6.8$ eV. Due to the nearly constant velocity one can also infer the origin of the ion burst. It starts at $t > 6\,\mu$s when the current rises *prior* to the formation of the fireball. Thus, the ions are ejected from the sheath as it changes from ion rich to electron rich when a positive voltage is applied [37]. The delay of $6\,\mu$s between voltage application and ion acceleration is longer than the ion transit time through the sheath. Thus, the initial sheath potential drop is only about 7 V for an applied voltage of 80 V. In time the sheath drop must increase; otherwise there could be no ionization and formation of a double layer. The subsequent ejection of newly produced ions was shown in figure 7.

3.5. Electron plasma oscillations

Double layers produce ion and electron beams both of which can create instabilities. The electron beam inside a fireball can potentially excite electron plasma waves. We have observed high-frequency oscillations inside a fireball, as shown in figure 10.

A pulsed fireball is created in Ar which is stable as indicated by the trace of electrode current. The electron saturation current shows a rise, a peak and a gradual decrease in density at $z = 0.5$ cm in front of the electrode. The temporary current loss at 35 μs is explained by a plasma potential rise. The Langmuir probe is then used as an rf probe by connecting it to a tuned rf amplifier. A sharp emission line is observed at $f = 136$ MHz. Its timing changes with frequency which can be interpreted as a change in the plasma frequency during the density build-up. Weaker emissions are also seen during the density decrease indicated by the Langmuir probe. If the

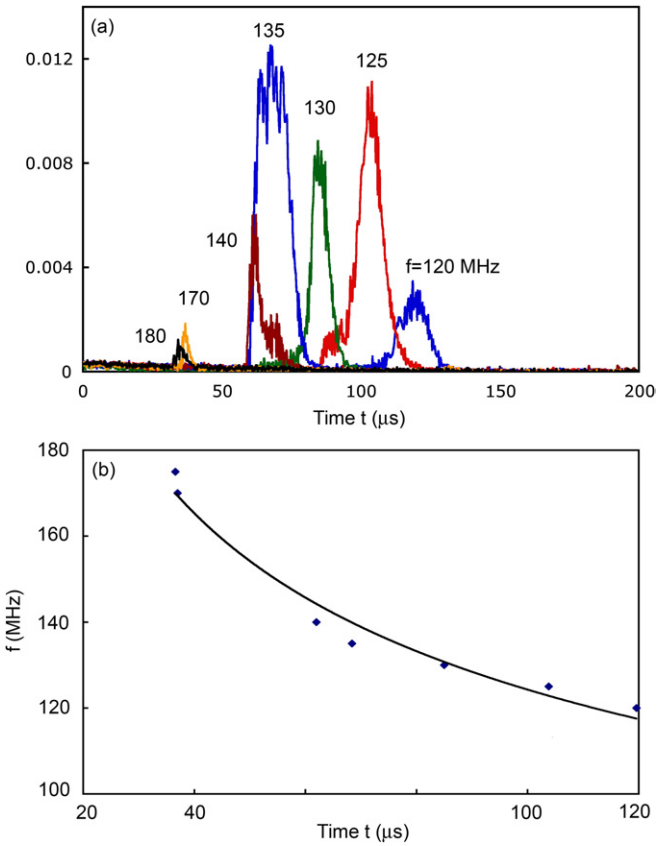

Figure 11. (*a*) Rf emission lines versus time at different frequencies. (*b*) Frequency versus time showing a decay due to a density drop in time.

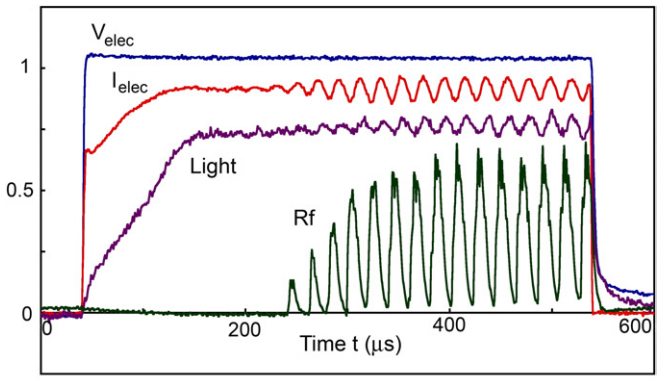

Figure 12. 100 MHz rf emission lines from a pulsed fireball which becomes weakly unstable in time. ($V_{elec} = 58$ V, $I_{elec,max} \simeq 150$ mA, $V_{dis} = 0$, $t_{pulse} = 0.5$ ms, $t_{rep} = 1.1$ ms, 2.8 mTorr Ar).

emission occurred at the plasma frequency these measurements would provide a precise density diagnostics.

Scanning the receiver frequency yields approximately the power spectrum of the emissions. Figure 11(*a*) displays emission lines in the frequency band from 120 to 180 MHz, outside of which the amplitudes become relatively small. There is a clear downshift in frequency with time, displayed in figure 11(*b*). Thus, during the pulsed fireball creation there is a density overshoot followed by a gradual density decrease, $\Delta n/n_{max} \simeq (1 - f^2_{p,min}/f^2_{p,max}) \simeq 0.55$ where $n_{max} \simeq 4 \times 10^8$ cm^{-3}.

When the fireball becomes unstable the emissions are modulated as shown in figure 12. The picture also shows that the emissions abruptly end when the fireball is switched off. The initial absence of emission lines must be that the plasma frequency does not match the receiver frequency.

After establishing that the rf emissions are temporally correlated with fireballs, i.e. the presence of electron beams, we now show that they are also spatially confined to the fireball. Figure 13(*a*) emission lines at a constant frequency (136 MHz) at different distances from the electrode. The lines shifts in time indicating some density non-uniformities even though the fireball is stable. The peak emission intensity versus axial distance is displayed in figure 13(*b*). The rf emission vanishes for $z > 2.5$ cm, i.e. outside the fireball. There is a peculiar axial distance ($z = 1.25$ cm) where no emission was seen at any time. This could be interpreted as a standing wave node. However, proper interferometry is needed to clarify the mode structure.

It is tempting to interpret the rf emissions as being due to electron beam–plasma instabilities. However, the relatively small size of the fireball and spherical geometry greatly complicate any comparison with theories usually formulated for one-dimensional uniform beam–plasma systems. If the electron beam had a velocity determined by a 15 eV double layer ($v_b \simeq 2.3 \times 10^8$ cm s^{-1}) the wavelength of a 100 MHz emission would be $\lambda = v_b/f_p \simeq 2$ cm which exceeds the radius of the fireball. The growth rate would have to be comparable to the frequency to produce the emission. The spherical geometry actually produces radially counter-streaming beams. The electron mean free path is larger than the fireball diameter such that many radially converging electrons will also radially diverge.

However, there is another possible explanation for the observed rf emissions: it has earlier been shown that an electron-rich sheath destabilizes the sheath–plasma resonance [12]. The mechanism is the finite electron transit time through a sheath which creates a negative differential resistance and can lead to oscillations of a resonant system such as the sheath–plasma resonance [25]. These oscillations have been observed on positively biased probes of various geometries and sizes. The high-frequency oscillation is often modulated by low-frequency instabilities as shown in figure 12. In order to distinguish the two excitation mechanisms the experiments would have to be done with larger or denser fireballs which accommodate many plasma wavelengths.

3.6. Magnetized fireballs

Fireballs have previously been observed and studied in magnetized plasmas [29, 35, 38]. The main effect is a change from spherical to cylindrical fireballs. The magnetization of electrons in uniform magnetic fields produces long firerods. The field-aligned dynamics is of particular interest.

In the present experiment we investigate pulsed fireballs in a dc dipole magnetic field which, for hydrogen, is strong enough to magnetize the ions. A samarium–cobalt magnet (2.5 cm diameter, 1 cm length, $B_{max} \simeq 2$ kG) is inserted into

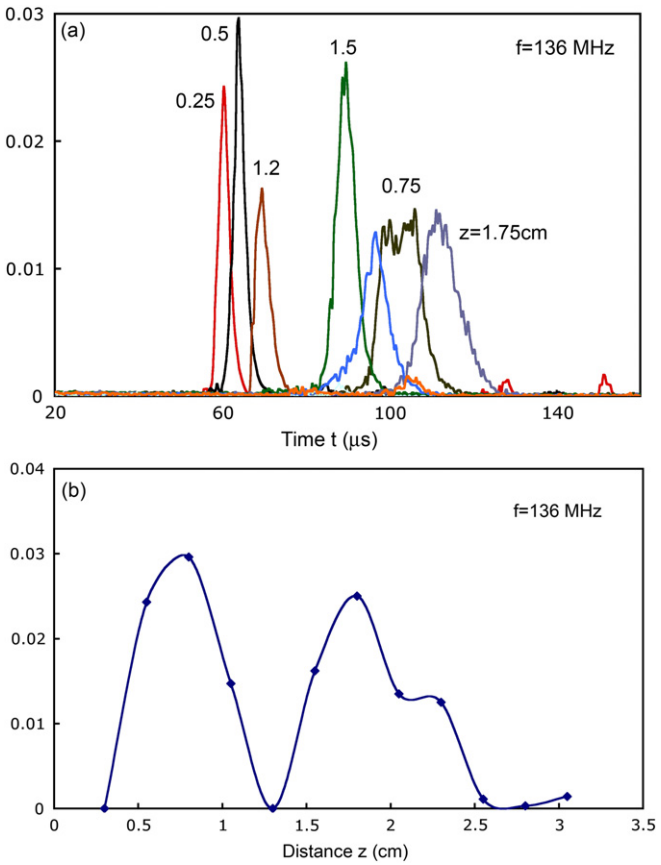

Figure 13. (*a*) Rf emission lines at a fixed frequency for different distances z from the electrode. (*b*) Peak rf intensity versus axial position indicating a mode pattern. Parameters as in figure 10.

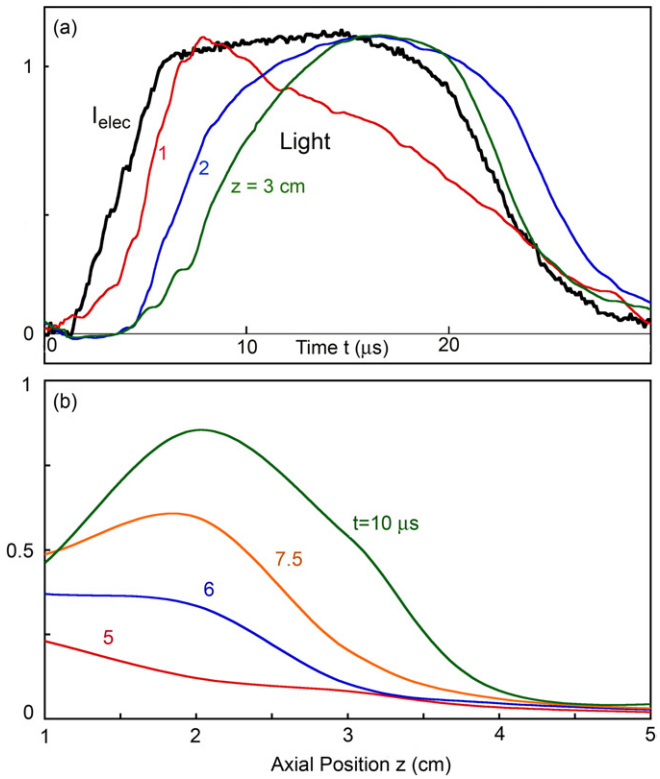

Figure 14. Time- and space-resolved light measurements of a pulsed argon fireball in front of a dipole magnet. (*a*) Electrode current waveform and normalized light intensity at different axial distances from the electrode (radial distance $\Delta r \simeq 3\,\mathrm{cm} = \mathrm{const.}$) Axial propagation occurs at ionic speeds, (*b*) Relative light intensity profiles at different times during the growth of the fireball. During the collapse the profile remains as for $t = 10\,\mu\mathrm{s}$ but decays in amplitude.

the plasma chamber. When the entire magnet was used as an electrode fireballs formed at uncontrolled locations. This was remedied by placing a disc electrode (1 cm diameter) in the front center of the floating magnet. Pear-shaped fireballs were produced as shown in figure 2(*d*). The spherical surface is the main region for electron acceleration. The cylindrical boundary is field-aligned, may have a large potential drop but cannot energize electrons across field lines. If the ions become unmagnetized they can be expelled across field lines. This can lead to periodic density depletions and current disruptions with or without ionization phenomena [5].

Using a photodiode movable inside the plasma chamber parallel to the fireball axis we have studied the space–time evolution of the light emission.

Figure 14(*a*) shows the waveforms of the unstable electrode current and the light emission at different axial distances from the electrode. The light intensity has been normalized to its temporal peak values so as to compare the waveforms. First, one can notice a pronounced delay between the onset of current and light. Thus the collected current is carried by low-energy electrons ahead of the double layer.

Next one observes that the delay increases with axial distance from the electrode in front of the magnet. Identifying the light emission via electron energization with a double layer, the latter propagates axially outwards during the current growth. Defining the propagation speed by the motion of the half-intensity point its value would be $\Delta z/\Delta t \simeq 2\,\mathrm{cm}/4\,\mu\mathrm{s} = 0.5\,\mathrm{cm}\,\mu\mathrm{s}^{-1}$, which is comparable to the speed of ballistic ions. Thus the growth of the double layer is controlled by the dynamics of the positive space–charge layer, i.e. the excess ions created by ionization in the parallel electric field.

Figure 14(*b*) addresses the absolute light intensity. It shows axial light intensity profiles at different times during the growth. Although the light starts at the electrode its absolute peak occurs at some distance from the electrode where the radius of the pear-shaped fireball is the largest. With further increasing distance ($z > 4\,\mathrm{cm}$) the light intensity rapidly drops off signifying the end of the fireball.

During the plateau of the electrode current the light profile becomes stationary. At $t \simeq 15\,\mu\mathrm{s}$ the current begins to decrease while $V_{\mathrm{elec}} = \mathrm{const}$. The light profile does not retract back to the electrode. It simply decays in position on a time scale comparable to or slower than the growth time.

In earlier observations of the same phenomenon (see figure 7(*b*) in [5]) the collapse was explained by depletion of neutrals, i.e. decrease in ionization to maintain the required ion flux to balance the collected electron flux. This appeared possible since the neutral pressure was lower while the collected current was three orders of magnitude higher ($I_{\mathrm{elec}} = 40\,\mathrm{A}$, 0.9 mTorr) than in the case. In this work the pump-out of neutrals due to ion fluxes appears negligible.

4. Conclusions

The dynamics of pulsed and unstable fireballs has been investigated experimentally. Observations of light, plasma parameters, particle bursts and waves help to understand the physics of fireball instabilities. The main observations are the following: when a positive voltage step ($\simeq$50 V) is applied to an electrode in a weakly ionized plasma the collected current shows a dramatic rise after a short delay. Light emission is produced by inelastic electron-neutral collisions requiring electron energies >15 eV. Ionization also occurs at this energy level. If an electron–ion pair is created in the sheath the electron is rapidly collected while the ion takes more time to be be accelerated away from the electrode. This leaves an excess positive space–charge layer in the originally electron-rich sheath. The double layer moves away from the electrode as the ions are accelerated. The increasing surface area of the double layer allows for larger electron currents to be collected from the background plasma which has certain limits. Extracting more electrons raises the plasma potential outside the fireball and lowers the double layer potential. The increasing surface decreases the expanding ion density which must be compensated by continuous ionization in the fireball although ions produced inside the fireball can expand only at the sound speed. Electrons produced inside the fireball cannot be collected faster than at the sound speed, hence are not responsible for the large current collection. Likewise the plasma production in the fireball does not increase the background density significantly due to the large volume ratio. The anode sheath must become ion rich to repel most secondary fireball electrons. A steady-state double layer requires momentum balance or a flux ratio $J_e/J_i = (m_i/m_e)^{1/2}$. If the electron flux is limited and the ion flux keeps growing the potential profile will change so as to limit the ion flux which requires a lowering of the double layer potential. This leads to another runaway phenomenon: as the double layer potential drops below the ionization potential the plasma production in the fireball stops. The density drops due to ion outflow. The density depression leads to a decrease in electron collection. The light of the fireball disappears. The cathode current may drop and the plasma production in the main chamber stops. In the meantime the current disruption re-establishes the initial conditions, i.e. a lower plasma potential and a large potential drop in the electrode sheath sufficient for ionization in the sheath. The process repeats as described in the beginning. Growth and collapse of the fireball can be considered runaway processes whose time scales are governed by ion transit times through the fireball. The recovery process depends on the density replenishment from the background plasma which may take longer due to a lower density and larger scales.

Now we explain the shapes of the fireball. It is well known that a stationary plane double layer requires momentum balance, $m_e n_e v_e = m_i n_i v_i$. Similarly, the entire fireball structure must be in force balance otherwise it would not be stationary structure. In a uniform, unmagnetized plasma this can only be accomplished with axially symmetric shapes where all radial forces cancel. The result are fireballs of spherical or cylindrical geometries. The axis of symmetry is normal to the electrode. At the point where the fireball touches the electrode the electron momentum is of course not balanced by ions, but the force on the electrode is too small to produce a noticeable recoil.

When an obstacle is inserted into the side of the fireball it is well known that the fireball moves away from the perturbation but remains spherical. The obstacle produces a local ion loss, reduces the ion momentum and creates a net force pushing the structure away from the obstacle. If the obstacle is a conductor biased positively to produce electron losses the fireball is attracted to the obstacle. The fireballs of two equally biased electrodes can merge into a cylindrical one stretching from one electrode to the other. It is not obvious how radially accelerated electrons with mean free path large compared with the fireball diameter can be collected at the ends of the firerod, unless an anomalous scattering process takes place inside the firerod. It has not been possible to create fireballs concentric to a spherical electrode, presumably due to reduced volume ionization. In a dipole magnetic field highly asymmetric fireballs exist off-axis because the field lines transfer the particle momentum to the magnet.

Acknowledgments

The work was partially supported by the Austrian Science Fund under Grant No L302-N02 and the University of Innsbruck. One of the authors (RLS) would like to thank the Experimental Plasma Physics Group at the University of Innsbruck for their kind hospitality during his stay in October 2007.

References

[1] Mott-Smith H M and Langmuir I 1926 The theory of collectors in gaseous discharges *Phys. Rev.* **28** 727–63
[2] Chen F F 1965 Electric probes *Plasma Diagnostic Techniques* ed R H Huddlestone and S L Leonard (New York: Academic) pp 113–200
[3] Sonmor L J and Laframboise J G 1991 *Phys. Fluids* B **3** 2472
[4] Bills D G, Holt R B and McClure B T 19652 Pulsed probe measurements *J. Appl. Phys.* **33** 29–33
[5] Stenzel R L and Urrutia J M 1997 Pulsed currents carried by whistlers: VIII. Electrode current disruptions by plasma erosion *Phys. Plasmas* **4** 26–35
[6] Bohm D, Durhop E H S and Massey H S W 1949 A Study of the Arc Plasma *Characteristics of Electrical Discharges in Magnetic Fields* ed A Guthrie and R K Wakerling (New York: Mc-GrawHill)
[7] Laframboise J G and Rubinstein J 1976 Theory of a cylindrical probe in a collisionless magnetoplasma *Phys. Fluids* **19** 1900–8
[8] Chen F F 2001 Langmuir probe analysis for high density plasmas *Phys. Plasmas* **8** 3029–41
[9] Stenzel R L, Ooyama M and Nakamura Y 1981 Potential double layers formed by ion beam reflection in magnetized plasmas *Phys. Fluids* **24** 708–18
[10] Armstrong R and Schrittwieser R 1991 Ion beam driven low frequency instability at a probe in a double-plasma device *Plasma Phys. Control. Fusion* **33** 1407–22
[11] Griskey M C and Stenzel R L 1999 Secondary-electron-emission instability in a plasma *Phys. Rev. Lett.* **82** 556–9
[12] Stenzel R L 1989 High-frequency instability of the sheath-plasma resonance *Phys. Fluids* B **1** 2273–82

[13] Stenzel R L 1978 Experiments on current-driven three-dimensional ion sound turbulence: II. Wave dynamics *Phys. Fluids* **21** 99–108
[14] Motley R W and D'Angelo N 1963 Excitation of electrostatic plasma oscillations near the ion cyclotron frequency *Phys. Fluids* **6** 296–9
[15] Sato N and Hatakeyama R 1985 A mechanism for potential-driven electrostatic ion cyclotron oscillations in a plasma *J. Phys. Soc. Japan* **54** 1661–4
[16] Popa G, Schrittwieser R, Rasmussen J J and Krumm P H 1985 The electrostatic ion-cyclotron instability—a two-dimensional potential relaxation instability *Plasma Phys. Control. Fusion* **27** 1063–7
[17] Urrutia J M and Stenzel R L 1997 Pulsed currents carried by whistlers: IX. In situ measurements of currents disrupted by plasma erosion *Phys. Plasmas* **4** 36–52
[18] Urrutia J M and Stenzel R L 1988 Transport of current by whistler waves *Phys Rev. Lett.* **62** 272–5
[19] Gekelman W and Vincena S 2005 Imaging complex three-dimensional alfven wave currents *IEEE Trans. Plasma Sci.* **33** 546–7
[20] Stenzel R L and Urrutia J M 1990 Currents between tethered electrodes in a magnetized laboratory plasma *J. Geophys. Res.* **95** 6209–26
[21] Stenzel R L, Gekelman W and Wild N 1982 Double layer formation during current sheet disruptions in a reconnection experiment *Geophys. Res. Lett.* **9** 680–3
[22] Torven S, Lindberg L and Carpenter R T 1985 Spontaneous transfer of magnetically stored energy to kinetic energy by electric double layers *Plasma Phys. Control. Fusion* **27** 143–58
[23] Nakamura Y, Nomura Y and Stenzel R L 1981 Sheath expansion of plane probe by ion-beam reflection *J. Appl. Phys.* **52** 1197–201
[24] Emeleus K G 1984 International journal of electronics *Plasma Phys. Control. Fusion* **56** 441–3
[25] Sanduloviciu M and Lozneanu E 1986 On the generation mechanism and the instability properties of anode double layers *Plasma Phys. Control. Fusion* **28** 585–95
[26] Song B, D'Angelo N and Merlino R L 1991 On anode spots, double layers and plasma contactors *J. Phys. D: Appl. Phys.* **24** 1789–95
[27] Conde L and Leon L 1994 Multiple double layers in a glow discharge *Phys. Plasmas* **1** 2441–7
[28] Gyergyek T, Cercek M, Schrittwieser R and Ionita C 2002 Experimental study of the creation of a firerod: I. Temporal development of the electron distribution function *Contrib. Plasma Phys.* **42** 508–25
[29] Gyergyek T, Cercek M, Schrittwieser R, Ionita C, Popa G and Pohoata V 2003 Experimental study of the creation of a firerod: II. Emissive probe measurements *Contrib. Plasma Phys.* **43** 11–24
[30] Dimitriu D G, Afliori M, Ivan L M, Ionita C and Schrittwieser R W 2007 Common physical mechanism for concentric and non-concentric multiple double layers in plasma *Plasma Phys. Control. Fusion* **49** 237–48
[31] Ionita C, Dimitriu D G and Schrittwieser R 2004 Elementary processes at the origin of the generation and dynamics of multiple double layers in dp machine plasma *Int. J. Mass Spectrom.* **233** 343–54
[32] Siebenfoercher A and Schrittwieser R 1996 A new simple emissive probe *Rev. Sci. Instrum.* **67** 849–50
[33] Andersson D 1981 Double layer formation in a magnetized laboratory plasma *J. Phys. D: Appl. Phys.* **14** 1403–18
[34] Cooke D and Katz I 1988 Ionization-induced instability in an electron-collecting sheath *J. Spacecraft and Rockets* **25** 132–8
[35] An T, Merlino R L and D'Angelo N 1994 Cylindrical anode double layers ('firerods') produced in a uniform magnetic field *J. Phys. D: Appl. Phys.* **27** 1906–13
[36] Pohoata V, Popa G, Schrittwieser R, Ionita C and Cercek M 2003 Properties and control of anode double layer oscillations and related phenomena *Phys. Rev.* E **68** 016405
[37] Schrittwieser R and Rasmussen J J 1982 Highly supersonic ion pulses in a collisionless magnetized plasma *Phys. Fluids* **25** 48–51
[38] Torven S and Andersson D 1979 Observations of electric double layers in a magnetized plasma column *J. Phys. D: Appl. Phys.* **12** 717–22